Available online at www.sciencedirect.com
ScienceDirect
Journal of Solid State Chemistry 180 (2007) 2643–2648
JOURNAL OF SOLID STATE CHEMISTRY
www.elsevier.com/locate/jssc

Order–disorder transition in $Nd_{2-y}Gd_yZr_2O_7$ pyrochlore solid solution: An X-ray diffraction and Raman spectroscopic study

B.P. Mandal[a], Ankita Banerji[b], Vasant Sathe[c], S.K. Deb[b], A.K. Tyagi[a,*]

[a]*Chemistry Division, Bhabha Atomic Research Centre, Mumbai 400085, India*
[b]*High Pressure Physics Division, Bhabha Atomic Research Centre, Mumbai 400085, India*
[c]*UGC-DAE CSR, University Campus, Khandwa Road, Indore 452 017, India*

Received 21 August 2006; received in revised form 6 July 2007; accepted 15 July 2007
Available online 20 July 2007

Abstract

Powder X-ray diffraction (XRD) and Raman spectroscopic study of order–disorder-phase transition with increase in the content of Gd in $Nd_{2-y}Gd_yZr_2O_7$ solid solution is being reported. It has been observed from Rietveld analysis that with increase in concentration of Gd in $Nd_{2-y}Gd_yZr_2O_7$, the value of the x parameter of the 48*f* oxygen changes from 0.332(1) to 0.343(1) with a sudden change in the slope for $y = 1.8$, which indicates that the structure is transforming from ordered pyrochlore to disordered pyrochlore. In addition to that a sudden and drastic change in the Raman spectra including changes in the position and width of several Raman modes beyond $y \geqslant 1.8$ has also been observed which has been correlated with increasing disorder. Based on these studies, it is suggested that there is a discontinuous order–disorder transition from 'perfect pyrochlore' to 'defect pyrochlore' phase in $Nd_{2-y}Gd_yZr_2O_7$ solid solution.

Keywords: Ceramics; X-ray diffraction (XRD); Raman spectroscopy

1. Introduction

Pyrochlore structure is cubic $Fd\bar{3}m$, ($Z = 8$, $a \approx 10$ Å), and the structural formula is ideally $^{VIII}A_2^{VI}B_2^{IV}X_6^{IV}Y$ (Roman numerals indicate the coordination number), where A is a trivalent rare earth ion, but can also be a mono, divalent cation and B may be 3*d*, 4*d* or 5*d* transition element having an appropriate oxidation state required for charge balance to give rise to the composition $A_2B_2O_7$ [1,2]. The pyrochlore structure is closely related to the fluorite structure AX_2, except that there are two cation sites and one-eighth of the anions are absent, as lucidly illustrated in Ref. [2].

Pyrochlore-structured compositions have a wide range of technologically important properties, such as high ionic conductivity [3], superconductivity [4], luminescence [5] and ferromagnetism [6]. In addition, zirconates are important ceramic waste forms for actinide immobilization and are among the principal host phases currently considered for the disposition of Pu from dismantled nuclear weapons [7].

New pyrochlores with varying radius ratio are of recent scientific interest. For the ordered pyrochlore, $A_2B_2O_7$, the phase stability of the superstructure is basically determined by the A and B site cation radius ratio. In view of this, there has been a considerable research interest in studying the phenomena of order–disorder-phase transition from pyrochlore ⇔ defect fluorite structure. At high temperatures some of the pyrochlore phases undergo order–disorder transition and change to disordered fluorite phases, which occur at, for example, ≈2300 °C for $Nd_2Zr_2O_7$ and at 2000 °C for $Sm_2Zr_2O_7$ [8]. It may be noted that the phase in which $A_2B_2O_7$ will crystallize also depends on the sample processing conditions [9]. It is worth noting here that the compounds with similar cationic radii are more likely to form as disordered fluorites than ordered pyrochlores, for instance, $Er_2Zr_2O_7$ having $r_A/r_B \approx 1.39$ crystallizes as a disordered fluorite structure whereas $Er_2Ti_2O_7$ with $r_A/r_B \approx 1.66$ crystallizes as a ordered pyrochlore structure [10]. In an attempt to explain various experimental observations of the order–disorder transitions in the

*Corresponding author. Fax: +91 22 2550 5151.
E-mail address: aktyagi@barc.gov.in (A.K. Tyagi).

0022-4596/$ - see front matter © 2007 Elsevier Inc. All rights reserved.
doi:10.1016/j.jssc.2007.07.007

pyrochlore system many groups [11–13] have calculated the defect formation energies of a large number of pyrochlore compositions. They suggested that the *B* site variation has relatively greater importance over the *A* site variation in determining the energetics of defect formation which was contradicted by Lian et al. [14]. Glerup et al. [15] have reported Rietveld analysis and Raman scattering on the series $Y_2Ti_{2-y}Zr_yO_7$ and they concluded that with increase in Zr content the system undergoes a structural change from the perfect pyrochlore structure to a defect fluorite structure through an intermediate disordered pyrochlore phase. In addition to fully ordered and fully disordered (defect fluorites) states, partially disordered state can also exist. In this investigation, an attempt has been made to vary the *A* site cations to systematically delineate the structural evolution leading to order–disorder transitions. Rietveld analysis was performed on the powder X-ray diffraction (XRD) patterns of the $Nd_{2-y}Gd_yZr_2O_7$ solid solutions and the results were supported by detailed Raman spectroscopic studies. To the best of our knowledge no spectroscopic studies are available on the substitution of Nd by Gd in $Nd_2Zr_2O_7$ in the literature. $Nd_{2-y}Gd_yZr_2O_7$ is an important system from the point of view of americium immobilization or transmutation as Nd is used as a surrogate material for Am. Both Nd^{3+} and Am^{3+} have same ionic radii [10] (1.02 Å in cubic coordination), which is an important criterion for simulation of phase relations.

2. Experimental details

AR grade Nd_2O_3, Gd_2O_3 and ZrO_2 were first heated at 900 °C for overnight to remove moisture and other volatile impurities. Stoichiometric amounts of the reactants were weighed to get the compositions corresponding to $Nd_{2-y}Gd_yZr_2O_7$. The homogenized mixtures were then subjected to a three-step heating protocol as follows with intermittent grindings. The thoroughly ground mixtures were heated in the pellet form at 1200 °C for 36 h, followed by a second heating at 1300 °C for 36 h after regrinding and repelletizing. In order to attain a better homogeneity, the products obtained after second heating were reground, pelletized and heated at 1400 °C for 48 h, which was the final annealing temperature for all the specimens. The heating and cooling rates were 2° per minute in all the annealing steps and atmosphere was static air. The XRD pattern of samples were recorded from $2\theta = 10$ to 90° on a Philips X'pert Pro XRD unit in static air condition with monochromatized Cu-$K\alpha$ radiation ($K\alpha_1 = 1.5406$ Å and $K\alpha_2 = 1.5444$ Å). The diffraction pattern is recorded in step scan mode with step width 0.02° and step time 3.30 s. Since XRD peaks were sharp and symmetric therefore the possibility of a secondary parasitic phase can be ruled out. Since the starting materials are high melting point solids, therefore to complete the reaction high temperature is required. The Raman spectra were recorded using a 632.8 nm line from a He–Ne laser and the scattered light was analyzed using a single-stage spectrograph (Horiba JY Model HR800). The laser was focused to a spot of ~5 μm and a 10× objective lens was used for the collection of back-scattered Raman signal. The instrument was calibrated before performing the measurement.

3. Results and discussion

The XRD patterns of all the products in $Nd_{2-y}Gd_yZr_2O_7$ ($0.0 \leqslant y \leqslant 2.0$) were recorded and analyzed. Some typical XRD patterns are shown in Fig. 1a–c. It has been found that, with increase in Gd^{3+} content the lattice parameter decreases (Table 1) continuously, which is attributed to the relative ionic size of Nd^{3+} and Gd^{3+}. This also established the monophasic nature of all the products in this series. Structural analysis has been done by using Rietveld refinement program Fullprof-2005 [16]. First of all, the background parameters and scale factor were adjusted. The background was fitted with sixth order polynomial. The diffraction peak profile was fitted with Pseudo-Voigt profile function and then the FWHM parameters were adjusted. No absorption parameter was considered during refinement. Subsequently, individual thermal parameters were refined. Finally, positional parameters were refined. The output of the refinement has been summarized in Table 1. The most important observation of the present investigation is that the 48*f* oxygen '*x*' parameter systematically increases with increase in Gd^{3+} content in this series. The variation of *x* parameter as a function of Gd content is shown in Fig. 2. The value of the *x* parameter increases on going from one end member $Nd_2Zr_2O_7$ to the other end member $Gd_2Zr_2O_7$. However, there is a distinct change in the slope at $Nd_{0.2}Gd_{1.8}Zr_2O_7$ composition. The implication of the sudden change in slope in the *x*-parameter vs. Gd-content curve will be explained later.

It has been shown by Dickson et al. [17] that the intensity of the (111) reflection is most sensitive to the position of the *x*-parameter of 48*f* oxygen. It is known that as the *x*-parameter approaches 0.375 (fluorite structure), the intensities of the characteristic pyrochlore XRD peaks approaches to zero, as given in Table 1 in which the relative intensity of (222) plane is 100% and with respect to that the intensity of (111) has been incorporated. This trend has been observed in $Nd_{2-y}Gd_yZr_2O_7$ series also (Fig. 1a–c) and also shown in Table 1. Originally, in pyrochlore structure all the oxygens are not equivalent. The oxygen at 48*f* position is surrounded by two *A* and two *B* cations and 8*a* position is having four *B* neighboring atoms, and 8*b* position is surrounded by four *A* cations. However, in pyrochlore structure, the 8*a* position is vacant, therefore, the 48*f* oxygen shifts from its ideal tetrahedral position towards two of its *B* cations. It has been observed after Rietveld analysis that with increase in the Gd content in $Nd_{2-y}Gd_yZr_2O_7$ series, the shift of 48*f* oxygen towards *B* cation decreases leading to increase in the *x*-parameter of 48*f* oxygen (*B* cation at origin) which drives the system to transform from ordered pyrochlore to disordered

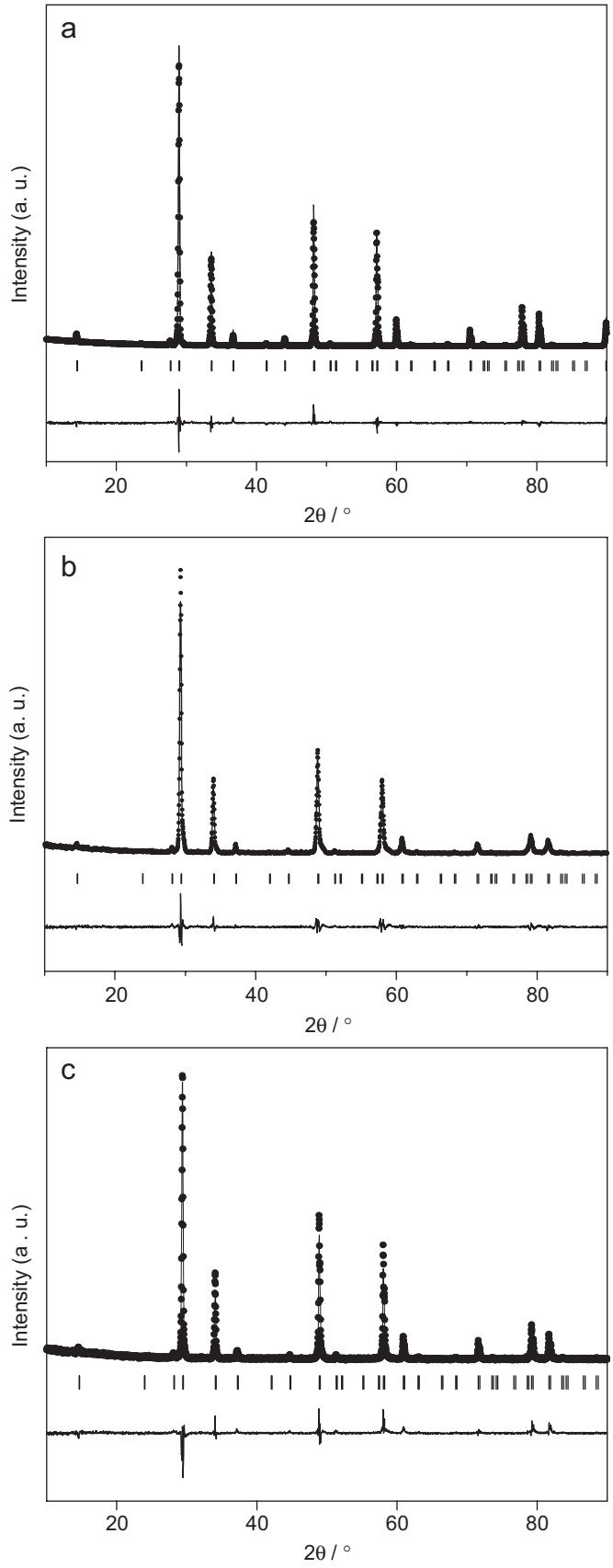

Fig. 1. (a) Observed and calculated XRD patterns of $Nd_2Zr_2O_7$; (b) observed and calculated XRD patterns $Nd_{0.15}Gd_{1.85}Zr_2O_7$ and (c) observed and calculated XRD patterns $Gd_2Zr_2O_7$.

pyrochlore and finally to defect fluorite. Ideally, in an ordered pyrochlore structure ($A_2B_2O_6O'$), the oxygen x parameter lies within the limit 0.3125–0.375 taking origin (0,0,0) at the B cation site [1]. At $x = 0.3125$, the B ion has a perfect octahedral coordination and 'A' cation resides at the centre of distorted hexagonal (six 48f O) network with two oxygens (8b O') perpendicular to the hexagonal plane. At $x = 0.375$, 'A' cation occupies the centre of regular cube and B cation will be at the center of highly distorted octahedron [18].

Pannetier [19] and Barker et al. [20] based on Madelung energy and site potential calculation, revealed that pyrochlores (3+, 4+ pyrochlore) with $x \approx 0.36$ may also exist but they have a tendency to easily transform to the defect fluorite structure. Therefore, it is not surprising to observe the disordered pyrochlore even when x is close to 0.36, in the present investigation. Recently, we [21] reported that for $Dy_2Hf_2O_7$ the x parameter is 0.348 and it crystallizes as a disordered pyrochlore. The x parameters of 48f oxygen of compositions from $Nd_{0.15}Gd_{1.85}Zr_2O_7$ to $Gd_2Zr_2O_7$, lying within the range 0.342(1)–0.344(1) which is very much susceptible to transformation into disordered pyrochlore.

XRD studies are more sensitive to disorder in the cationic sublattice compared to anionic sublattice whereas Raman spectroscopy is primarily sensitive to oxygen-cation vibrations and is an excellent probe for local disorder. The Raman spectroscopic investigation has been found to provide unequivocal information [15] to distinguish between a pyrochlore, disordered pyrochlore and a defect-fluorite material, because these phases differ essentially with respect to local disorder around the A or B cations. Therefore, all the compounds were further investigated by Raman spectroscopy over the frequency range 200–800 cm^{-1} to investigate the exact composition at and beyond which a distinct pyrochlore lattice undergoes a transformation to disordered pyrochlore.

Pure $Nd_2Zr_2O_7$ crystallizes in pyrochlore structure with space group $Fd\bar{3}m$. The six Raman active modes are distributed as $A_{1g} + E_g + 4F_{2g}$ [22]. The Raman spectrum of the pyrochlore structure of $Nd_2Zr_2O_7$ and the different mode frequencies agree quite well with the values reported in the literature [23]. Only difference is that Vandenborre [24] et al. had observed two distinct modes at 523 and 532 cm^{-1}, whereas we observe a broad peak, which could be resolved into two components at 506 and 531 cm^{-1} using least-squares fitting with two lorentzian. All the lines in the Raman spectrum are quite broad, which is due to inherent disorder in the system. The XRD peaks are quite sharp and narrow, which indicate the size of the particles are in micro-region. Thus, the broadening due to smaller particle size can be ruled out. Our earlier low temperature Raman study [25] does not show any significant changes in the width of the lines, which implies that the origin of broad line shape is not due to anharmonic effect but is primarily due to disorder. This can be clearly seen from the Raman spectra of $Nd_2Zr_2O_7$ and $Gd_2Zr_2O_7$, where the line width for the latter compound is much larger than the

Table 1
Important parameters of different compositions of $Nd_{2-y}Gd_yZr_2O_7$ series

	2.0	1.95	1.85	1.8	1.6	0.4	0.0
Lattice parameter (A)	10.5406(8)	10.5429(2)	10.5433(4)	10.5571(5)	10.5688(14)	10.6092(8)	10.6801(6)
Total number of independent reflection	39	39	39	39	39	39	39
Gd ion (16*d*) (0.5,0.5,0.5) B (A^2)	0.4(1)	0.5(1)	0.4(1)	0.5(1)	0.4(1)	0.6(1)	
Nd ion (16*d*) (0.5,0.5,0.5) B (A^2)		0.5(1)	0.4(1)	0.5(1)	0.4(1)	0.6(1)	0.51(6)
Zr ion (16*c*) (0,0,0) B (A^2)	1.4(1)	1.3(1)	1.4(1)	1.0(1)	1.0(1)	1.1(1)	0.9(1)
Fractional coordinate, x	0.344(1)	0.343(1)	0.342(1)	0.340(1)	0.338(1)	0.334(2)	0.332(1)
O1 ion (48*f*) (x, 0.125,0.125) B (A^2)	1.9(7)	1.6(4)	1.7(7)	1.1(4)	1.9(4)	1.6(4)	1.5(3)
O2 ion (8*b*) (0.125,0.125, 0.125) B (A^2)	0.60(4)	0.64(6)	0.78(7)	0.51(7)	0.52(6)	0.54(4)	0.43(4)
DW-stat	0.9020	1.0326	0.9334	1.2860	0.9183	0.9998	0.9642
R_p	7.65	6.65	6.01	8.25	7.62	6.56	7.74
R_{wp}	9.6	9.27	8.36	9.80	9.87	9.59	10.2
R_{exp}	6.28	6.21	5.39	6.77	6.55	6.55	7.65
χ^2	2.33	2.23	2.40	2.10	2.27	2.14	1.77
A–O bond distance	2.483(3)	2.492(4)	2.499(3)	2.511(2)	2.518(4)	2.582(3)	2.584(4)
B–O bond distance	2.110(3)	2.105(3)	2.100(4)	2.094(4)	2.087(7)	2.081(5)	2.081(3)
$I_{(111)}$ /$I_{(222)}$ (%)	0.33	0.56	0.91	1.63	1.86	2.53	3.19

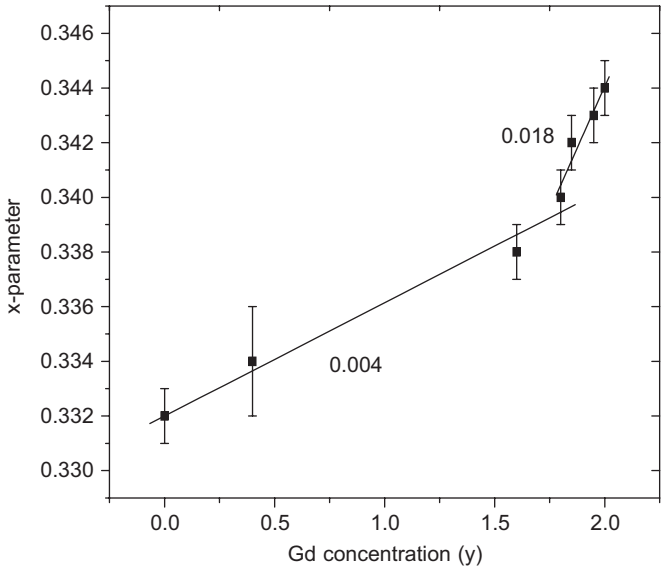

Fig. 2. Variation of x parameter of 48*f* oxygen with concentration of Gd in $Nd_{2-y}Gd_yZr_2O_7$ series.

former even though both the compounds belong to the same pyrochlore phase [1]. It has been argued that even in an ordered compound there is considerable disorder in the form of vacancy, defects and presence of 'foreign' atoms/ions (for alloys and mixed systems), which breaks down the translational periodicity of the lattice and hence relaxes the $k \approx 0$ selection rule. Thus there is contribution from non zone-center phonons which can lead to line broadening for a phonon branch for which there is considerable dispersion over the Brillouin zone. Since all the Raman active vibrations involve oxygen motion the origin of broadening is mainly due to structural disorder present in the system due to existence of random vacancy from the statistical nature of the oxygen occupancy among various sites. The assignment of the different modes to corresponding

Table 2
Raman mode frequencies with symmetry character and vibration types

Frequency (cm^{-1})	Symmetry	Vibration type
305	F_{2g}	Zr–O6 bending
399	E_g	Mostly Zr–O strech with mixture of Nd–O strech and O–Zr–O bending vibrations
506	A_{1g}	Mostly O–Zr–O bend with mixture of Zr–O and Nd–O stretch
523	F_{2g}	Mostly O–Zr–O bend
594	F_{2g}	Mostly Zr–O strech

vibrations is a non-trivial task in the absence of a single crystal and polarized Raman spectra. Most of the assignments have been done based on lattice dynamical calculation in different systems [26–29] and they are shown in the Table 2. Fig. 3 shows the changes in the Raman spectra with increasing concentration of Gd in the system and it can be seen that with increase in the doping proportion of Gd in $Nd_2Zr_2O_7$, the width of all the Raman lines increases till it is extremely broad for the $Gd_2Zr_2O_7$ end member. We also observe intensity redistribution among the modes at 521 and 590 cm^{-1} for $y \geqslant 1.2$ As the content of Gd increases, the two nearby modes at 506 and 523 cm^{-1} become extremely broad and could not be resolved into two separate modes and finally merge with each other. The most interesting observation is that the intensity of the strong characteristic pyrochlore Raman mode at $\approx 305\,cm^{-1}$ gradually diminishes and there is considerable broadening of the mode. Fig. 4 shows the changes in the frequency of different modes (ω) with increasing proportion of Gd (y) and it can be seen that there is very little change in the peak position of different modes which is primarily due to the fact that the these modes involve movement of oxygen ions, but not the Gd or Nd ions. However, we notice a change in the slope for the ω–y curve for all the lines when the Gd concentration (y) exceeds 1.8.

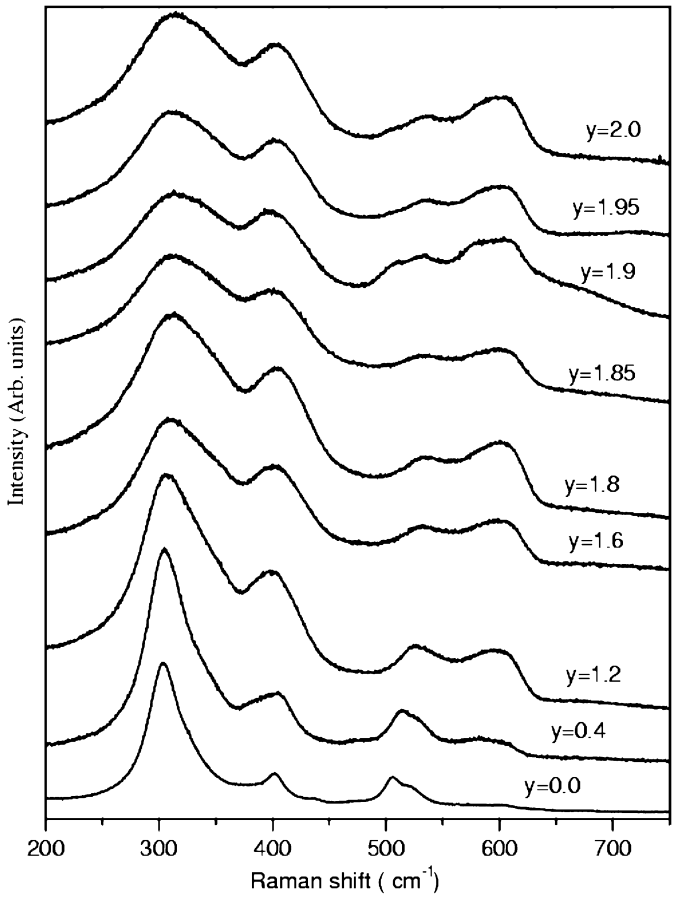

Fig. 3. Raman spectra of $Nd_{2-y}Gd_yZr_2O_7$ with increasing proportion of Gd: (a) $Nd_2Zr_2O_7$, (b) $Nd_{1.2}Gd_{0.8}Zr_2O_7$, (c) $Nd_{0.8}Gd_{1.2}Zr_2O_7$, (d) $Nd_{0.4}Gd_{1.2}Zr_2O_7$, (e) $Nd_{0.2}Gd_{1.8}Zr_2O_7$, (f) $Nd_{0.15}Gd_{1.85}Zr_2O_7$, (g) $Nd_{0.1}Gd_{1.9}Zr_2O_7$, (h) $Nd_{0.05}Gd_{1.95}Zr_2O_7$ and (i) $Gd_2Zr_2O_7$. This figure shows the spectra over 200–800 cm^{-1} representing vibration modes.

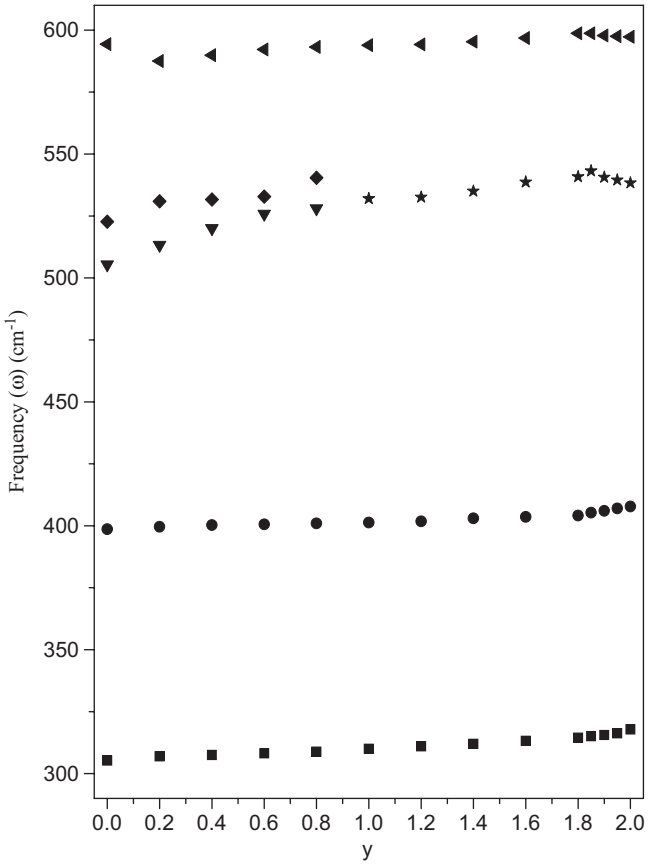

Fig. 4. Change in the frequency of different modes (ω) with increasing proportion of Gd in $Nd_{2-y}Gd_yZr_2O_7$ series.

The width of different modes also increases with increasing Gd concentration. The changes in width for two of the modes at 305 and 399 cm^{-1} can be seen in Fig. 5 which clearly shows sudden change in the slope beyond $y = 1.8$. In order to understand the changes in the Raman spectrum we refer to Fig. 2 where the value of the x parameter of the 48f oxygen position is plotted as a function of the Gd concentration. We observe a gradual increase in the x parameter till $y \approx 1.8$ beyond which there is sudden change in the slope even though the radius ratio r_A/r_B changes linearly. The change in slope observed in the ω–y curve and the sudden increase in width in the Raman modes for $y \geqslant 1.8$ can be related to this discontinuous change in the x parameter. As the size difference between "average" A cation and B cation decreases with increase of Gd content, the system has a tendency to transform from perfect pyrochlore to defect pyrochlore. The oxygen vacancy, which was ordered in perfect pyrochlore, gets gradually randomized with increase in Gd content. This is evident from Raman spectra of several pyrochlore [8], and there is direct correlation between the value of the x-parameter of the 48f oxygen and the width of the different Raman modes. For x values closer to the perfect pyrochlore phase the width is less and as the x parameter increases the width increases. This is directly related to the cationic antisite disorder leading to the oxygen disorder, which increases the width of the Raman lines. Glerup et al. [14] had used Raman spectroscopy to investigate the transition from perfect pyrochlore to disordered fluorite phase in $Y_2Ti_{2-y}Zr_yO_7$ system with increasing y. They have shown that with increasing y the Raman spectrum becomes broader till $y = 0.9$ when it is in a defect pyrochlore phase, however the qualitative nature of the spectrum remains unchanged. On the other hand for $y = 1.4$ they claim the phase to be defect fluorite. They also show spectra for several yttria-stabilized-Zirconia (YSZ), in disordered fluorite phase with different amount of Y substitution. Our system is different than that for Glerup et al., in the sense that we consider the case where the A cation is being continuously substituted between the two end members. In addition to change in the x parameter, we observe change in A^{3+}–O and B^{4+}–O distances also and here too we observed sudden changes beyond $y \approx 1.8$ and since the mode frequencies depend on these distances we observe corresponding changes in the ω–y curve. All these changes observed in the XRD and Raman spectrum of the $Nd_{2-y}Gd_yZr_2O_7$ solid solution beyond $y \approx 1.8$ lead us to

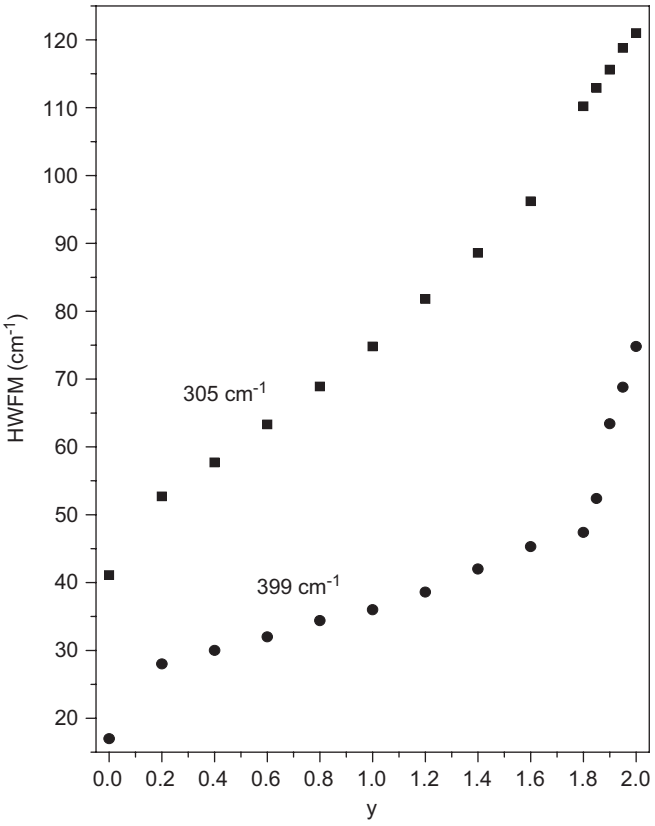

Fig. 5. The changes in width for two of the modes (305 and 399 cm^{-1}) with Gd content in $Nd_{2-y}Gd_yZr_2O_7$ series.

conclude that the 'pyrochlore' system shows a discontinuous transition to 'defect pyrochlore' phase beyond a Gd concentration of $y = 1.8$.

4. Conclusion

The solid solution $Nd_{2-y}Gd_yZr_2O_7$ shows complete homogeneity range with continuous change in the lattice constant and with increase in Gd content in the lattice, the r_A/r_B ratio deceases continuously as the distinction between A and B sites reduces which further drives to form antisite defects and this causes local oxygen disorder which is evidenced by increased width of the Raman modes. However the most important observation is the discontinuous nature of the transition beyond a certain concentration of Gd whereby the system transforms from ordered pyrochlore to disordered pyrochlore structure. Another significant conclusion can be drawn that A site variation is also important for order–disorder transition supporting the observation of Lian et al. [14]. The exact composition at which the ordered pyrochore gets transformed to disordered pyrochlore structure could be unequivocally delineated by plotting 'x' parameter as a function of Gd-content as well as using Raman spectroscopy.

Acknowledgment

Authors are very much thankful to Dr. P.S.R. Krishna and Dr. S. Mishra, BARC for their help in Rietveld refinement.

References

[1] M.A. Subramanian, G. Aravamudan, G.V. Subba Rao, Prog. Solid State Chem. 15 (1983) 55.
[2] W.R. Panero, L. Stixrude, R.C. Ewing, Phys. Rev. B 70 (2004) 054110.
[3] B.J. Wuensch, K.W. Eberman, C. Heremans, E.M. Ku, P. Onnerud, E.M.E. Yeo, S.M. Haile, J.K. Stalick, J.D. Jorgensen, Solid State Ionics 129 (2000) 111.
[4] J. Yamaura, Y. Muraoka, F. Sakai, Z. Hiroi, J. Phys. Chem. Solids 63 (2002) 1027.
[5] J.K. Park, C.H. Kim, K.J. Choi, H.D. Park, S.Y. Choi, J. Mater. Res. 16 (2001) 2568.
[6] M.J.P. Gingras, B.C. den Hertog, M. Faucher, J.S. Gardner, S.R. Dunsiger, L.J. Chang, B.D. Gaulin, N.P. Raju, J.E. Greedan, Phys. Rev. B 62 (2000) 6496.
[7] R.C. Ewing, W.J. Weber, J. Lian, J. Appl. Phys. 95 (2004) 5949.
[8] D. Michael, M. Perez, Y. Jorba, R. Collongues, J. Raman Spectrosc. 5 (1976) 163.
[9] G.L. Catchen, T.M. Rearick, Phys. Rev B 52 (1995) 9890.
[10] R.D. Shanon, Acta Crystallogr. A 32 (1976) 751.
[11] M. Pirzada, R.W. Grimes, L. Minervini, J.F. Maguire, K.E. Sickafus, Solid State Ionics 140 (2001) 201.
[12] K.E. Sickafus, L. Minervini, R.W. Grimes, J.A. Valdez, M. Ishimaru, F. Li, K.J. McClellan, T. Hartmann, Science 289 (2000) 748.
[13] P.J. Wilde, C.R.A. Catlow, Solid State Ionics 112 (1998) 173.
[14] J. Lian, J. Chen, L.M. Wang, R.C. Ewing, J.M. Farmer, L.A. Boatner, K.B. Helean, Phys. Rev. B 68 (2003) 134107.
[15] M. Glerup, O.F. Nielsen, F.W. Poulsen, J. Solid State Chem. 160 (2001) 25.
[16] WinPLOTR, J Rodríguez-Carvajal, Laboratorie Leon Brillouin (CEA-CNRS), April 2005 (LLB-LCSIM).
[17] S.J. Dickson, K.D. Hawkings, T.J. White, J. Solid State Chem. 82 (1986) 146.
[18] J.M. Longo, P.M. Raccah, J.B. Goodenough, Mater. Res. Bull. 4 (1969) 191;
H.S. Horowitz, J.M. Longo, J.T. Lewandowski, Mater. Res. Bull. 16 (1981) 489.
[19] J. Pannetier, J. Phys. Chem. Solids 34 (1973) 583.
[20] W.W. Barker, P.S. White, O. Knop, Can. J. Chem. 54 (1976) 2316.
[21] B.P. Mandal, N. Garg, S.M. Sharma, A.K. Tyagi, J Solid State Chem. 179 (2006) 1990.
[22] M.T. Vandenborre, E. Husson, J.P. Chatry, D. Michel, J. Raman Spectrosc. 14 (1983) 63.
[23] N.V. Gundovin, F.M. Spiridonov, L.N. Komissarova, K.I. Petrov, Russ. J. Inorg. Chem. 20 (1975) 325.
[24] N.T. Vandenborre, E. Husson, H. Brusset, Spectrochim. Acta 37A (1981) 113.
[25] Ankita Banerji, T.N. Sairam, C.S. Sunder, S.K. Deb, Proc. Solid State Symp. 51 (2006) 149.
[26] B.E. Scheetz, W.B. White, J. Am. Ceram. Soc 62 (1979) 468.
[27] H.C. Gupta, S. Brown, J. Phys. Chem. Sol. 64 (2003) 2205.
[28] H.C. Gupta, S. Brown, N. Rani, V.B. Gohel, Int. J. Inorg. Mater. 3 (2001) 983.
[29] S. Brown, H.C. Gupta, J.A. Alonso, M.J. Martinez-Lope, J. Raman Spectrosc. 34 (2003) 240.